Response to Reviewer 2 Comments

Thank you for your decision and constructive comments on my manuscript. We have revised the manuscript carefully according to the reviewers' comments. Point–to–point responses are given below. The original comments are black in color, while our responses are in blue. The revised parts in the manuscript are marked in red. All the page number and line number are referred to the revised manuscript.

Major concerns:

Point 1: How to interpret the variations of low ozone concentrations / background ozone for the targeted region as it's surrounded by polluted areas?

Response 1: In principle, the lowest daily O_3 concentrations usually occur before sunrise due to nighttime titration of NO, and the low percentile (2^{nd}) usually characterizes baseline or background conditions because increases in the low O_3 percentile tend to be associated with increases in baseline or background O_3 concentrations. Similar conclusions were also obtained from both models and observations (Jacob et al., 1999; Cynthia Lin et al., 2000). Li et al. (2014) reported that concentrations below the 5^{th}, between 25^{th} and 75^{th}, and above 95^{th} represent background, typical, and polluted concentrations, respectively. Thus, in our manuscript, low O_3 concentration levels were determined by the 2^{nd} percentiles of hourly O_3 concentrations in each month for cities in eastern China (Li et al., 2022; Cooper et al., 2012; Gaudel et al., 2020). Based on the 2^{nd} O_3 percentile concentrations, we explore the driving forces of the low O_3 trends in eastern China in recent years. Firstly, the Multiple Linear Regression (MLR) model is used to evaluate the anthropogenic and meteorological contributions to the 98^{th} and 2^{nd} O_3 percentile trends. Then, we discuss the impacts of meteorological factors and anthropogenic emissions on low O_3 concentrations, including the impact of the COVID–19 pandemic, and sustained heatwave of extremely hot and dry summer in eastern China in 2022, respectively, and detailed information can be found in the discussion section of the manuscript.

Point 2: How to identify the ozone formation sensitivity based on FNR (ratio of formaldehyde and NO_2).

Response 2: This method belongs to one of the photochemical indicator diagnostics of O_3 formation sensitivity (Chu et al., 2024), and the FNR is the ratio of the volume concentration of HCHO to NO_2. HCHO is a transient product reflecting the oxidation of various VOCs, serving as a proxy for VOCs emissions, as used in previous studies (Zheng et al., 2018; Zhang

et al., 2019). The ratio of NO_2 to NO in NO_x is relatively constant, and the NO_2 concentration can represent the evolution process of atmospheric NO_x. Therefore, HCHO and NO_2 can be taken as representatives of VOCs and NO_x, respectively. This photochemical indicator was originally derived from the photochemical indicator HCHO/NO_y (the ratio of HCHO and NO_y volume concentrations). Jin et al. (2017) suggested that FNR is better suited than HCHO/NO_y for determining O_3 formation sensitivity because both HCHO and NO_2 have short lifetimes (about a few hours), and their ratios can better represent the competition between OH radicals and the reaction between VOCs and NO_2.

This photochemical indicator has been widely used not only in the analysis of ground–based observations, but also in satellite observations, and Martin et al. (2004) were the first to propose the diagnosis of O_3 formation sensitivity based on satellite observations of FNR. Currently, this method has been refined and extended to various O_3 monitoring instrument products (Ren et al., 2022; Chang et al., 2016), such as OMI (Ozone Monitoring Instrument), TROPOMI (Tropospheric Monitoring Instrument) and GEMS (Geostationary Environment Monitoring Spectrometer).

The reliability of surface FNR in the diagnosis of O_3 formation sensitivity was recently assessed by Liu et al. (2021). Based on a joint analysis of multiple in situ observations and model simulations, the validity of FNR in diagnosing O_3 formation sensitivity was determined based on the relative changes in O_3 generation rates with respect to several indicators. Lin et al. (2022) further extended the FNR to the vertical distribution and diagnosed the O_3 formation sensitivity at different altitude using vertical profile of NO_2 and HCHO observed by Multi-Axis Differential Absorption Spectrometer (MAX–DOAS), and the methodology employed in our manuscript is consistent with that of Lin et al (2022).

The advantage of this method is that O_3 formation sensitivities can be quickly determined from photochemical indicators. However, the threshold value of FNR is always the core problem in the application of this method, and its threshold value will change with different environmental conditions, especially the thresholds in different regions tend to differ greatly. Therefore, there are differences in the thresholds reported in different literatures.

Three steps are involved in determining the FNR_{sec} threshold. First, the surface–hourly averaged secondary HCHO and NO_2 VMRs during May–September based on MAX–DOAS observations were normalized by dividing their respective mean values because of the large differences in surface HCHO and NO_2 concentrations (Ren et al., 2022). The ratio of the hourly averaged O_3 VMRs to the hourly averaged normalized NO_2 VMRs (S_{NO2}) and the ratio of the hourly averaged O_3 VMRs to the hourly averaged normalized secondary HCHO VMRs (S_{HCHO})

were calculated. Finally, third–order polynomials were used to fit S_{NO2} and S_{HCHO} (Fig. R1). When S_{NO2} is significantly larger than S_{HCHO}, O_3 formation is more sensitive to NO_x (larger FNR_{sec}), which is the NO_x–limited regime, and vice versa. For example, in Hefei, S_{NO2} and S_{HCHO} intersected at FNR_{sec}=0.21. FNR_{sec} less than 0.16 and greater than 0.29 correspond to VOC–limited regime and NO_x–limited regime, respectively, where the relative difference between S_{NO2} and S_{HCHO} is more than 25% (Lin et al., 2022), and the range of FNR_{sec} from 0.16 to 0.29 represents a transition regime.

In addition, following the referee's suggestion, the manuscript was edited by Elsevier Language Editing Services (please see the following Elsevier certificate).

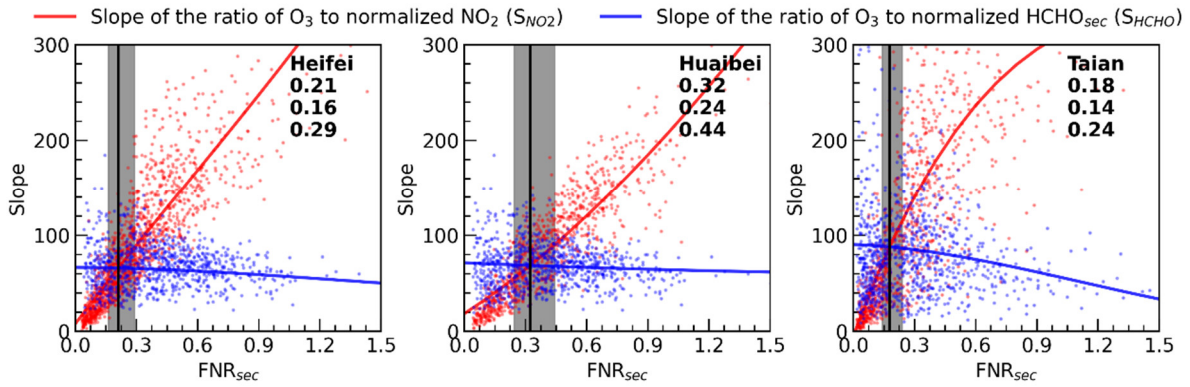

Fig.R1. Three–order fitting of slopes of O_3 VMRs versus normalized NO_2 VMRs and slopes of O_3 VMRs versus normalized secondary HCHO VMRs in different FNR_{sec} values in Hefei, Huaibei, and Tai'an during May–September based on MAX–DOAS observations. The intersect at FNR_{sec} indicated by the black solid line. The vertical shadow indicates the relative difference between the slopes of O_3 VMRs versus normalized NO_2 VMRs and slopes of O_3 VMRs versus secondary HCHO VMRs within 25% (transition regime). The labels at the top right of each panel represent the intersect FNR_{sec} values and the thresholds for the NO_x–limited regime (high) and VOC–limited regime (low) in Hefei, Huaibei, and Tai'an, respectively.

Fig. R2 Certificate of Elsevier language editing services

Detailed comments:

1. Page 1, Line 27: in the main text, you mainly work on "HRB", instead of the whole eastern China. Maybe specifying HRB, instead of eastern China makes more sense.

Thanks for your suggestion. This study attempts to reveal the surface low and peak O_3 trends in eastern Chinese cities in recent years, and to explore the driving forces behind these trends. The surface observations show that the decreased trend in low O_3 concentrations and increased trend in peak O_3 concentrations are widespread in urban agglomerations in eastern China. In the original manuscript, we first analyzed the trend of low and peak O_3 values in the HRB, which were then extended to eastern China. In fact, we conducted MAX–DOAS measurements in three cities in eastern China, namely Hefei, Huaibei and Tai 'an (Fig.R3). First, the three cities are located at similar longitudes with large differences in latitude, transitioning sequentially from south to north. Secondly, the O_3 concentrations of the three cities differed greatly, with Tai' an having a higher surface mean MDA8 O_3 concentration (82.9 ppb), Hefei having a lower surface mean MDA8 O_3 concentration (65.5 ppb), and Huaibei having an intermediate surface mean MDA8 O_3 concentration (74.3 ppb). Therefore, Hefei, Huaibei and Tai 'an can be taken as representative of the 105 cities in eastern China to conduct O_3 precursor observations. In the new manuscript, we have deleted the analysis of the HRB and reorganized the manuscript.

The new manuscript mainly includes four parts. First, we report long–term records of surface O_3 and related parameters observed at urban air quality monitoring sites and by satellites in eastern China, characterizing the trends of low, typical, and peak surface O_3

concentrations during the warm season (May–September) from 2017 to 2022. Then, a Multiple Linear Regression (MLR) model is used to evaluate the anthropogenic and meteorological contributions to the 98th and 2nd O_3 percentile trends. Next, secondary formaldehyde (HCHO) and NO_2 are employed to diagnose the diurnal variations in O_3 formation sensitivity and investigate the reasons for peak O_3 concentration trends in the context of current NO_x reduction. Finally, we discuss the reasons for the potential increase in low O_3 concentrations and the sensitivity of peak and low O_3 trends during the study period. Please refer to our new manuscript for details.

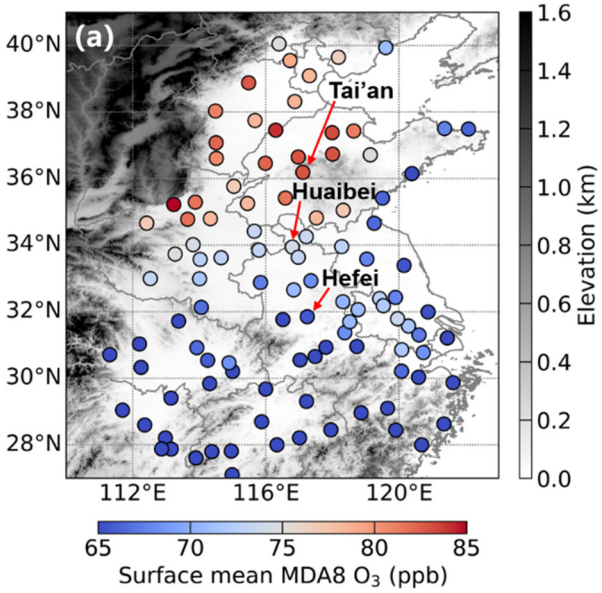

Fig.R3. Spatial distributions of surface mean MDA8 O_3 concentrations during May–September 2017–2022. The red arrow indicates the name of each city, which are equipped with ground–based MAX–DOAS observations

2. Page 1, Line 29: can you elaborate more on the "typical" ozone concentrations?

Thanks for your suggestion. We have followed this suggestion and elaborated more on the "typical" O_3 concentrations. "The decline in typical O_3 concentrations is notably slower than that of peak O_3 concentrations, approximately -0.02 ppb/year (-0.0% per year) during the same period.". Please refer to Page 1 Line 31–32 in the manuscript.

3. Page 1, Line 31: please rephrase the sentence. "Anthropogenic emissions" is not the "cause" of the ozone trends, maybe "driving force" is better.

Thanks for pointing out the unsuitable expression. We have followed this suggestion and corrected it. Please refer to Page 1 Line 33 in the manuscript.

4. Page 2, Line 3: change “on spatial scales” to “spatially”.

Thanks for pointing out the unsuitable expression. We have followed this suggestion and removed relevant expressions base on the new abstract.

5. Page 3, Line 5: duplicate reference of Li et al., 2020a

Thanks for pointing out the inappropriate quote, we have corrected it.

6. Page 5, line 18: have you applied consistent AMF (air mass factor) between MAX–DOAS and TROPOMI for NO_2 VCDs?

We did not apply consistent AMF (air mass factor) between MAX–DOAS and TROPOMI for NO_2 VCDs. NO_2 VCDs observed by TROPOMI was downloaded directly from https://search.earthdata.nasa.gov/search (last access: 1 July, 2024). The AMF calculation for MAX–DOAS is a two–step process that first retrieve the atmospheric aerosol vertical profile and then inputs the aerosol vertical profile into the radiative transfer model SCIATRAN, to compute the atmospheric photon paths that are used to convert the NO_2 slanting column concentration into a vertical column concentration (Xing et al., 2017).

7. Page 5, Line 21: why the differences of sensitivity peaks between TROPOMI and MAX-DOAS lead to different HCHO VCD retrievals?

TROPOMI is a space–borne instrument to observe the atmospheric trace gas column concentration from the top down, while MAX–DOAS is a ground–based spectrometer to observe the atmospheric trace gas column concentration from the bottom up. TROPOMI sensitivity peaks in the upper troposphere, which rapidly drops in the atmospheric layers lower than 3 km (Vigouroux et al., 2020), while MAX–DOAS shows an opposite sensitivity that is maximal at the surface and generally becomes negligible above 3 km (De Smedt et al., 2021; Wang et al., 2019). The HCHO concentrations usually concentrated below 2 km over the polluted city (Fig.R4). Therefore, TROPOMI may underestimate the HCHO concentration below 3 km, resulting in a smaller retrieved HCHO VCD. Similar comparative results are also seen in other cities around the world (De Smedt et al., 2021).

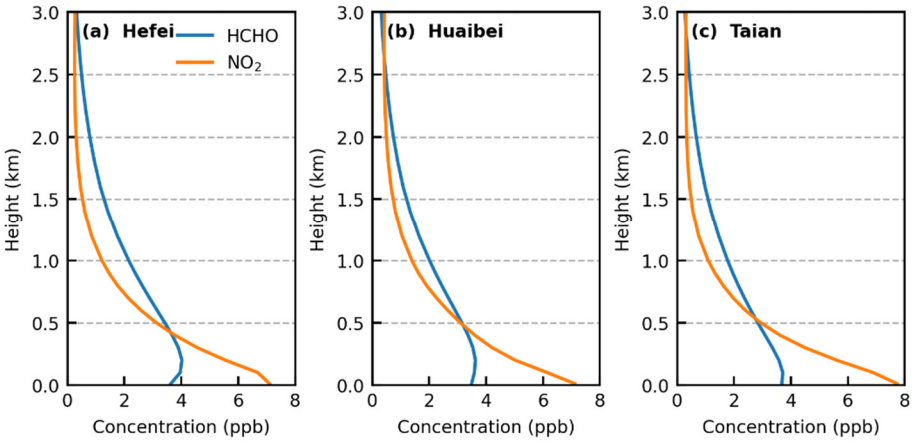

Fig.R4. Mean profiles of NO_2 and HCHO concentrations in (a) Hefei, (b) Huaibei, and (c) Tai'an during the whole observation period from May to September.

8. Page 5, Line 24-26: so, what's the conclusion? Are MAX-DOAS data not reliable compared to MEE, as the correlation coefficients are not that high (0.66~0.74)? Please specify it.

The MAX–DOAS data are reliable. Although the correlation coefficients are not that high (0.66~0.74), were also comparable to the comparisons reported in previous studies (Lin et al., 2022; Wang et al., 2020). The differences between MAX–DOAS and MEE observations arise from these two components. First, there was a difference in the detection geometries, as the urban NO_2 concentration observed by MAX–DOAS was the result of scanning along a certain direction, whereas the urban NO_2 concentration observed by MEE was sampled in situ. Second, there were some differences in their locations, and the urban NO_2 concentration of the MEE was the average of several in–situ observation stations (10, 3, and 3 in Hefei, Huaibei, and Tai'an, respectively), whereas we only used one MAX–DOAS in each city. We have added this statement to the manuscript, please refer to Page 5 Line 4–10.

9. Page 6, line 27: this is not true for summer, as VOCs can be dominated by biogenic sources.

Thanks for pointing out the unsuitable expression. We have followed this suggestion and removed relevant expressions.

10. Page 6, Line 28: how about transport from surrounding areas? Especially in HRB, the transport cannot be neglected as it's surrounded by the YRD and Jing-Jin-Ji regions. Please elaborate more.

The effect of transport is included in the meteorological factors, and we considered the effect of horizontal transport (wind speed of u and v components) as well as vertical exchange rates

(vertical velocity at 850 hPa) in MLR fitting. The results also show that horizontal winds and vertical exchange rates are also a key meteorological factor affecting O_3 concentrations in many cities in eastern China (Table R1 and R2). The effect of horizontal winds can be seen in two aspects, one is that strong winds blow away high concentrations of O_3 and its precursors, and the other is that they bring high concentrations of O_3 and its precursors. We also discuss this result in detail in the Discussion section of the manuscript as well. Please refer to Page 14 Line 20–30.

Table R1. Meteorological drivers of 2% O_3 percentile and Pearson correlation coefficient between observed and modeled 2% O_3 percentile in each city of eastern China during May–September 2017–2022

	Meteorological variable					Meteorological variable			
	1st	2st	3st	R		1st	2st	3st	R
Taian	T	RH	U	0.35	Beijing	U	RH	T	0.23
Puyang	T	BLH	RH	0.50	Tianjing	U	T	RH	0.32
Rizhao	U	V	T	0.46	Baoding	U	RH	TP	0.27
Jining	RH	T	V	0.54	Lanfang	U	T	V	0.23
Xinxiang	U	RH	V	0.41	Shijiazhuang	RH	BLH	U	0.27
Jiaozuo	T	RH	U	0.39	Handan	RH	V	BLH	0.20
Heze	RH	T	V	0.47	Qinghuangdao	V	U	RH	0.32
Linyi	RH	U	TP	0.40	Cangzhou	BLH	T	MSLP	0.28
Kaifeng	RH	U	T	0.49	Xingtai	RH	BLH	U	0.17
Zhengzhou	BLH	RH	U	0.47	Hengshui	T	V	RH	0.28
Luoyang	BLH	RH	V	0.16	Tangshan	U	V	RH	0.20
Zaozhuang	RH	T	U	0.46	Jinan	V	BLH	RH	0.59
Lianyungang	RH	V850	U	0.37	Qingdao	V	BLH	RH	0.26
Shangqiu	RH	T	V	0.48	Zibo	V	BLH	RH	0.59
Xuzhou	RH	BLH	V	0.48	Dongying	U	V	V850	0.36
Xuchang	BLH	RH	U	0.53	Yantai	V	BLH	U	0.33
Suqian	RH	T	MSLP	0.40	Weifang	BLH	T	U	0.34
Huaibei	RH	U	BLH	0.59	Weihai	RH	U	MSLP	0.36
Pingdingshan	BLH	RH	U	0.57	Dezhou	RH	V	BLH	0.40
Bozhou	RH	V	T	0.49	Liaocheng	BLH	V	RH	0.48
Zhoukou	RH	U	T	0.49	Binzhou	BLH	T	V	0.23
Luohe	RH	U	MSLP	0.45	Shaoxing	RH	BLH	T	0.59
Suzhou	RH	U	BLH	0.50	Jinhua	RH	TP	V	0.60
Huaian	RH	V	TP	0.42	Taizhou	V	RH	U	0.54
Yancheng	V	RH	BLH	0.37	Ningbo	RH	V	TP	0.48
Nanyang	RH	U	BLH	0.67	Wuhan	RH	V	BLH	0.61
Zhumadian	RH	TP	BLH	0.52	Changsha	RH	V	BLH	0.71
Fuyang	RH	V	U	0.64	Jinghzou	RH	V	BLH	0.55
Bengbu	RH	BLH	U	0.36	Yueyang	RH	BLH	V	0.60
Huainan	RH	BLH	U	0.56	Zhuzhou	RH	V	BLH	0.73
Xinyang	RH	TP	T	0.63	Xiangtan	RH	V	BLH	0.72
Suizhou	RH	BLH	U	0.63	Yichang	RH	U	V850	0.64
Shanghai	RH	V	TP	0.55	Yiyang	RH	V	BLH	0.67
Nanjing	V	RH	T	0.40	Changde	V	BLH	RH	0.59
Wuxi	RH	V	BLH	0.57	Jingmen	V	RH	U	0.63
Changzhou	V	RH	TP	0.49	Huangshi	RH	U	V850	0.72
Suzhou	RH	V	T	0.52	Huanggang	RH	U	V850	0.77
Nantong	V	RH	U	0.62	Xianning	RH	U	MSLP	0.74

Yangzhou	V	RH	T	0.52	Xiaogan	RH	V850	BLH	0.68
Zhenjiang	V	RH	T	0.55	Quzhou	V	RH	U	0.68
Taizhou	V	RH	T	0.59	Lishui	RH	V	T	0.70
Luan	RH	V	T	0.24	Wenzhou	RH	V	U	0.63
Hangzhou	RH	V	BLH	0.53	Jiujiang	V	RH	MSLP	0.58
Jiaxing	RH	V	T	0.45	Nanchang	V	RH	V850	0.67
Huzhou	V	RH	U	0.61	Jingdezhen	BLH	V850	T	0.59
Hefei	RH	TP	V	0.37	Shangrao	V850	BLH	RH	0.65
Wuhu	V	TP	U	0.46	Yingtan	BLH	V850	RH	0.64
Maanshan	V	U	TP	0.45	Yichun	V850	U	T	0.63
Tonglin	V	T	TP	0.50	Fuzhou	RH	V	BLH	0.72
Anqing	V	T	TP	0.56	Jian	BLH	U	RH	0.57
Chuzhou	RH	V	BLH	0.44	Xinyu	BLH	V	U	0.62
Chizhou	RH	V	BLH	0.47	Pingxiang	V850	BLH	T	0.61
Xuancheng	T	RH	U	0.27	-	-	-	-	-

Table R2. Meteorological drivers of 98% O_3 percentile and Pearson correlation coefficient between observed and modeled 98% O_3 percentile in each city of eastern China during May–September 2017–2022

	Meteorological variable					Meteorological variable			
	1st	2st	3st	R		1st	2st	3st	R
Taian	T	TP	TCC	0.71	Beijing	MSLP	BLH	V	0.30
Puyang	T	V850	TP	0.79	Tianjing	V	MSLP	BLH	0.27
Rizhao	T	U	TCC	0.67	Baoding	MSLP	V	BLH	0.28
Jining	T	TP	V850	0.77	Lanfang	MSLP	BLH	V	0.32
Xinxiang	T	TCC	BLH	0.74	Shijiazhuang	MSLP	BLH	V	0.24
Jiaozuo	T	TP	TCC	0.81	Handan	T	MSLP	U	0.31
Heze	T	V850	TP	0.78	Qinghuangdao	TCC	U	MSLP	0.36
Linyi	T	TP	TCC	0.73	Cangzhou	V	BLH	MSLP	0.35
Kaifeng	T	V850	TP	0.78	Xingtai	MSLP	BLH	V	0.25
Zhengzhou	T	V850	TP	0.78	Hengshui	V	MSLP	BLH	0.38
Luoyang	U	TCC	V	0.28	Tangshan	TCC	MSLP	T	0.27
Zaozhuang	T	TP	TCC	0.81	Jinan	T	TP	V850	0.77
Lianyungang	TCC	U	TP	0.68	Qingdao	U	BLH	RH	0.45
Shangqiu	T	TP	V850	0.71	Zibo	T	TP	V850	0.70
Xuzhou	T	TCC	TP	0.74	Dongying	T	RH	V	0.66
Xuchang	T	V850	TCC	0.70	Yantai	U	T	RH	0.44
Suqian	RH	TCC	TP	0.74	Weifang	T	TP	U	0.68
Huaibei	TCC	T	TP	0.74	Weihai	U	T	RH	0.44
Pingdingshan	T	V850	U	0.66	Dezhou	T	TP	V850	0.75
Bozhou	TCC	T	TP	0.67	Liaocheng	T	V850	TP	0.77
Zhoukou	T	TCC	RH	0.73	Binzhou	T	TP	V	0.66
Luohe	T	V850	RH	0.75	Shaoxing	T	V	TP	0.66
Suzhou	TCC	T	TP	0.71	Jinhua	T	V	TP	0.59
Huaian	T	TCC	TP	0.72	Taizhou	U	V	T	0.62
Yancheng	TP	V850	U	0.56	Ningbo	T	V	U	0.69
Nanyang	T	TCC	RH	0.74	Wuhan	TCC	RH	V850	0.75
Zhumadian	TCC	BLH	TP	0.67	Changsha	RH	TCC	V	0.76
Fuyang	RH	TCC	MSLP	0.74	Jinghzou	RH	V850	T	0.84
Bengbu	T	TCC	TP	0.72	Yueyang	RH	TCC	U	0.82
Huainan	TCC	RH	MSLP	0.68	Zhuzhou	RH	V	T	0.73
Xinyang	RH	TCC	U	0.74	Xiangtan	RH	V	TCC	0.78
Suizhou	RH	TCC	MSLP	0.75	Yichang	RH	TCC	V850	0.79
Shanghai	T	U	RH	0.72	Yiyang	RH	TCC	V850	0.80
Nanjing	TCC	V850	V	0.61	Changde	TCC	V850	T	0.74
Wuxi	TP	TCC	U	0.66	Jingmen	RH	V850	T	0.76

Changzhou	TCC	TP	BLH	0.60	Huangshi	RH	TCC	V	0.76
Suzhou	T	TP	U	0.63	Huanggang	TCC	RH	U	0.72
Nantong	T	RH	BLH	0.75	Xianning	RH	V850	T	0.80
Yangzhou	TCC	TP	V850	0.61	Xiaogan	RH	TCC	U	0.72
Zhenjiang	TCC	TP	MSLP	0.61	Quzhou	RH	V850	T	0.74
Taizhou	TCC	V850	U	0.61	Lishui	RH	U	V	0.65
Luan	TCC	MSLP	T	0.61	Wenzhou	U	RH	V	0.65
Hangzhou	TP	TCC	T	0.69	Jiujiang	TCC	V850	RH	0.80
Jiaxing	T	TP	U	0.70	Nanchang	RH	V850	T	0.72
Huzhou	TP	TCC	T	0.67	Jingdezhen	RH	V850	TCC	0.75
Hefei	TCC	TP	V	0.59	Shangrao	TCC	V850	T	0.76
Wuhu	TCC	TP	V	0.65	Yingtan	TCC	V850	T	0.78
Maanshan	TCC	TP	MSLP	0.66	Yichun	V850	TCC	T	0.75
Tonglin	TCC	MSLP	V	0.63	Fuzhou	V850	T	TCC	0.82
Anqing	TCC	V	TP	0.58	Jian	TCC	T	V	0.66
Chuzhou	TCC	TP	MSLP	0.58	Xinyu	V850	TCC	V	0.75
Chizhou	TCC	V	MSLP	0.63	Pingxiang	V850	TCC	V	0.75
Xuancheng	TCC	V	MSLP	0.58	-	-	-	-	-

11. Page 7, Line 7: so, the perturbations of background ozone are neglected when considering the observed O_3 anomalies. It's not true as transport can contribute to this term.

We thank the reviewer for pointing out this issue. We are also aware of this issue, so we have corrected the MLR model in the manuscript. The updated MLR model first de–seasonalizes the O_3 concentration time series to remove meteorological variability in O_3 concentration. Following Liu et al. (2023) and Li et al. (2020), the MLR model fitted the deseasonalized and detrended 10 d mean 98th or 2nd O_3 percentile time series to the deseasonalized and detrended 10 d mean meteorological variables. The deseasonalized and detrended time series data were constructed by removing the 50 d moving average data from the 10 d moving average data. The stepwise MLR model has the following form:

$$Y(t) = R + \sum_{k=1}^{n} \beta_k X_k(t) \quad (1)$$

Where $Y(t)$ is the deseasonalized and detrended daily surface 98th or 2nd O_3 percentile time series, R is the regression constant, β_k is the regression coefficient, and X_k is the deseasonalized and detrended daily meteorological variable considered as a possible O_3 covariate. Stepwise regressions were performed, adding and removing terms based on their independent statistical significance to obtain the best model fit.

Daily meteorological variables were obtained from the ERA5 reanalysis data (Download from https://cds.climate.copernicus.eu, last access: January 7, 2024), included temperature (T, °C), surface relative humidity (RH, %), total cloud cover (TCC), total precipitation (TP, mm), mean sea level pressure (MSLP, hPa), wind speed of U, V components (U, V, m/s), boundary layer height (BLH, m), and vertical velocity at 850 hPa (V850, m/s).

First, we used the MLR model to remove the effects of meteorological variability from the 2017 to 2022 98th or 2nd O_3 percentile trends. We apply Eq. (1) to the meteorological anomalies X_k during May–September 2017–2022, obtained by removing the 6–year means of the 50 d moving averages from the 10 d mean time series. The anomalies calculated in this process were deseasonalized but not detrended. This yields the meteorology–driven 98th or 2nd O_3 percentile anomalies $Y_m(t)$

$$Y_m(t) = R + \sum_{k=1}^{n} \beta_k X_k(t) \quad (2)$$

Secondly, to avoid overfitting, only the three most important meteorological parameters were selected based on their individual contributions to the regressed 98th or 2nd O_3 percentiles, along with the requirement that they be statistically significant above the 95% confidence level in the MLR model (Li et al., 2018). The fit results and selected meteorological variables varied by city but were regionally consistent (Table R1 and Table R2). The 98th or 2nd O_3 percentile anomalies $Y_a(t)$ obtained by deseasonalizing, but not detrending, the 98th or 2nd O_3 percentile time series in a similar manner as for the meteorological variables (by removing the 6–year means of the 50 d moving averages). The residual anomaly $Y_r(t)$ after removing the meteorology–driven 98th or 2nd O_3 percentile anomalies from the MLR model is given by

$$Y_r(t) = Y_a(t) - Y_m(t) \quad (3)$$

Finally, the residual is an anomalous component that cannot be explained by the MLR meteorological model and is referred to as meteorologically corrected data by (Zhai et al., 2019). It consists of noise due to the limitations of the MLR model and other factors and can be mainly attributed to long–term trends in anthropogenic emission changes over a 6–year period. The trend in the regressed 98th or 2nd O_3 percentile reflected the meteorological contribution, and the residual was then used to reflect the presumed anthropogenic contribution. For the updated MLR model, please refer to section 2.4 in the manuscript.

12. Page 8, Line 2: HRB is surrounded by very polluted area, and it can be affected by pollution transport. It's hard to define "background" here, and the background concentrations can change interannually.

We agree with this suggestion, and this is one of the errors in the separation of primary and secondary sources of HCHO by Regression Model. We have extensively reviewed previous studies, and most of the literature has set the background concentration of HCHO at 1 ppb (Sun et al., 2021; Hong et al., 2018; Lin et al., 2022). In addition, according to the ground–level

measurements of HCHO at a rural site in the eastern China by Ma et al. (2016) and Wang et al. (2015), the background level of HCHO near the surface was approximately 1.0 ppb. Therefore, we used this background concentration (1 ppb) in our regression model. Moreover, The fitting results of the regression model are also comparable to those in the previous literature (Hong et al., 2018), so we consider the separation of the primary and secondary sources of HCHO in the manuscript to be reliable.

13. Page 10, line 5: how about the variations in the background?

We have corrected the MLR model in the manuscript (refer to 11). The natural background O_3 concentration is deducted before the stepwise multiple regression. Following Liu et al., (2023) and Li et al. (2020), the natural background O_3 concentration obtained by the 6–year means of the 50 d moving averages from the 10 d mean time series. The new manuscript focuses on the drivers of trends in peak (98^{th}) and low (2^{nd}) O_3 concentrations.

14. Page 10, line 28: do you include nighttime O_3 data in the MLR model? Why?

It is included nighttime O_3 data in the MLR model. This study attempts to reveal the surface low, typical, and peak O_3 trends in eastern Chinese cities in recent years, and to explore the driving forces behind these trends. The 2^{nd} and 98^{th} percentiles of hourly O_3 concentrations in each month for cities in eastern China were calculated to determine their long–term trends at low and peak concentration levels, respectively (Li et al., 2022; Cooper et al., 2012; Gaudel et al., 2020). In principle, the lowest daily O_3 concentrations usually occur before sunrise due to nighttime titration of NO, and the low percentile (2^{nd}) usually characterizes baseline or background conditions because increases in the low O_3 percentile tend to be associated with increases in baseline or background O_3 concentrations.

15. Page 11, Line 2: "(0.108 ppb/year, +114%)", what's this for?

It is the contribution of anthropogenic components on 2^{nd} O_3 percentiles trends. We updated the MLR model in the manuscript, rearranged section 3.2, and removed this description.

16. Page 11, line 27-28: This is weird. When S_{no2} is much larger than S_{hcho} (low FNR), it should be VOC-limited, instead of NOx-limited.

As shown in Fig.R1, the red and blue line represents the S_{NO2} and S_{HCHO}, respectively. When S_{NO2} is much larger than S_{HCHO}, the FNR is higher, and the O_3 formation is more sensitive to NO_x, which is NO_x–limited regime.

17. Figure 6: How do you calculate the slope of the ratio of O_3 to S_{no2}, and the slope of the ratio of O_3 to S_{hcho}? Are you using the ground measurements for all years? Does each point represent the fitted slope each day? I'm curious the temporal intervals between datapoints shown here.

First, the surface–hourly averaged secondary HCHO and NO_2 VMRs during May–September based on MAX–DOAS observations were normalized by dividing their respective mean values because of the large differences in surface HCHO and NO_2 concentrations. The ratio of the hourly averaged O_3 VMRs to the hourly averaged normalized NO_2 VMRs (S_{NO2}) and the ratio of the hourly averaged O_3 VMRs to the hourly averaged normalized secondary HCHO VMRs (S_{HCHO}) were calculated. Finally, third–order polynomials were used to fit S_{NO2} and S_{HCHO} (Fig.R1). S_{HCHO} and S_{NO2} were calculated using data from the warm season (May–September) for all years of MAX–DOAS observations, and each point in Fig.R1 in the manuscript represents the slope for each hour, and the temporal intervals is one hour between datapoints shown in Fig.R1 in the manuscript. We have added this statement to the manuscript, please refer to Page 11 Line 22–27 in the manuscript.

18. Figure 6: I'm curious will the FNR threshold change year by year based on this methodology? How will the interannual variation of the threshold affect your analyses? Please elaborate more.

Differences in the thresholds of the FNR at different times or regions are due to differences in the sources of the corresponding indicator species, whose thresholds vary with environmental conditions (Liu et al., 2021). We calculated the FNR thresholds separately according to different years, and it can be found that the differences in FNR thresholds in different years are very small (FigR5–R7), and the differences in FNR thresholds are mainly between different cities. Therefore, the interannual variation in the threshold have little effect on the results in our manuscript.

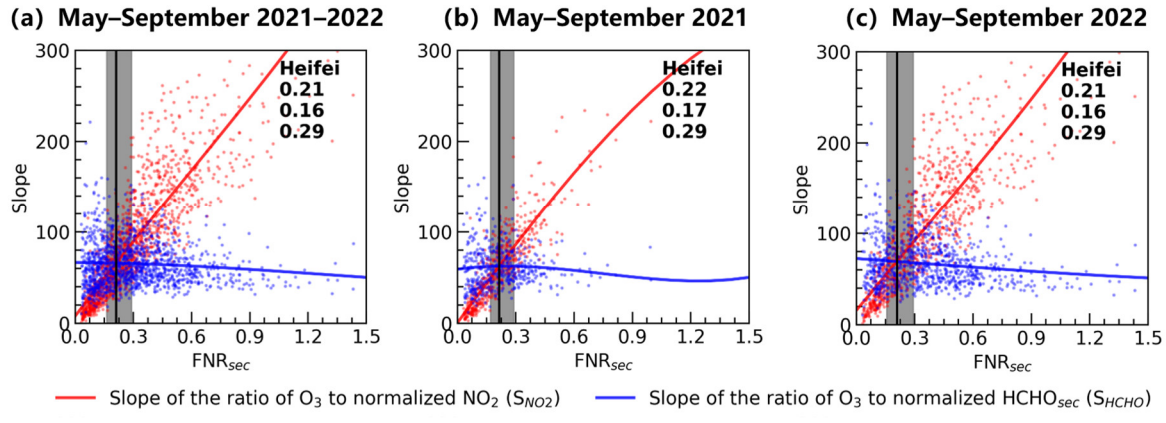

Fig.R5. Three–order fitting of slopes of O_3 VMRs versus normalized NO_2 VMRs and slopes of O_3 VMRs versus normalized secondary HCHO VMRs in different FNR_{sec} values in Hefei, during (a) May–September 2021–2022, (b) May–September 2021, and (c) May–September 2022.

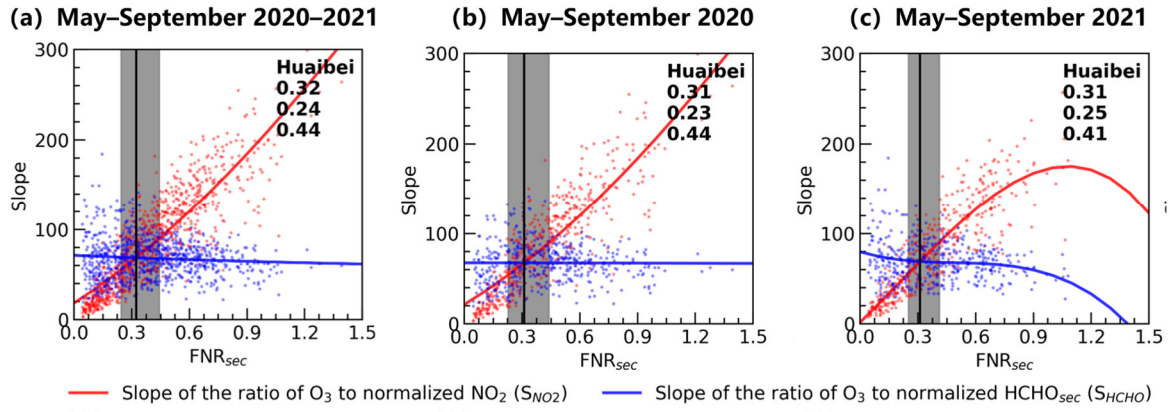

Fig.R6. Three–order fitting of slopes of O_3 VMRs versus normalized NO_2 VMRs and slopes of O_3 VMRs versus normalized secondary HCHO VMRs in different FNR_{sec} values in Huaibei, during (a) May–September 2020–2021, (b) May–September 2020, and (c) May–September 2021.

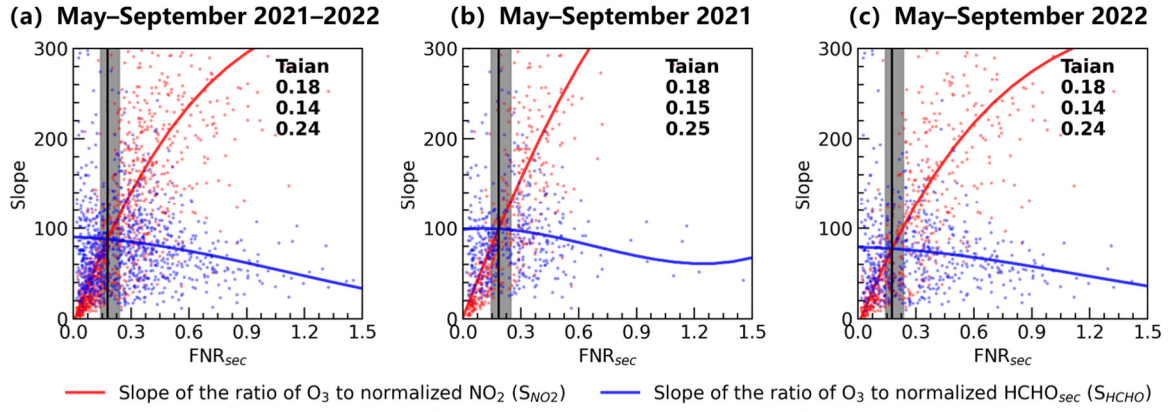

Fig.R7. The same as Fig.R5 but in Tai'an.

Reference:

Chang, C.-Y., Faust, E., Hou, X., Lee, P., Kim, H. C., Hedquist, B. C., and Liao, K.-J.: Investigating ambient ozone formation regimes in neighboring cities of shale plays in the Northeast United States using photochemical modeling and satellite retrievals, Atmos. Environ., 142, 152-170, 10.1016/j.atmosenv.2016.06.058, 2016.

Chu, W., Li, H., Ji, Y., Zhang, X., Xue, L., Gao, J., and An, C.: Research on ozone formation sensitivity based on observational methods: Development history, methodology, and application and prospects in China, J. Environ. Sci-China, 138, 543-560, 10.1016/j.jes.2023.02.052, 2024.

Cooper, O. R., Gao, R. S., Tarasick, D., Leblanc, T., and Sweeney, C.: Long‐term ozone trends at rural ozone monitoring sites across the United States, 1990–2010, J. Geophys. Res-atmos., 117, 10.1029/2012jd018261, 2012.

Cynthia Lin, C. Y., Jacob, D. J., Munger, J. W., and Fiore, A. M.: Increasing background ozone in surface air over the United States, Geophys. Res. Lett., 27, 3465-3468, 2000.

De Smedt, I., Pinardi, G., Vigouroux, C., Compernolle, S., Bais, A., Benavent, N., Boersma, F., Chan, K.-L., Donner, S., Eichmann, K.-U., Hedelt, P., Hendrick, F., Irie, H., Kumar, V., Lambert, J.-C., Langerock, B., Lerot, C., Liu, C., Loyola, D., Piters, A., Richter, A., Rivera Cárdenas, C., Romahn, F., Ryan, R. G., Sinha, V., Theys, N., Vlietinck, J., Wagner, T., Wang, T., Yu, H., and Van Roozendael, M.: Comparative assessment of TROPOMI and OMI formaldehyde observations and validation against MAX-DOAS network column measurements, Atmos. Chem. Phys., 21, 12561-12593, 10.5194/acp-21-12561-2021, 2021.

Gaudel, A., Cooper, O. R., Chang, K.-L., Bourgeois, I., Ziemke, J. R., Strode, S. A., Oman, L. D., Sellitto, P., Nédélec, P., and Blot, R.: Aircraft observations since the 1990s reveal increases of tropospheric ozone at multiple locations across the Northern Hemisphere, Sci. Adv., 6, eaba8272, 2020.

Hong, Q., Liu, C., Chan, K. L., Hu, Q., Xie, Z., Liu, H., Si, F., and Liu, J.: Ship-based MAX-DOAS measurements of tropospheric NO2, SO2, and HCHO distribution along the Yangtze River, Atmos. Chem. Phys., 18, 5931-5951, 10.5194/acp-18-5931-2018, 2018.

Jacob, D. J., Logan, J. A., and Murti, P. P.: Effect of rising Asian emissions on surface ozone in the United States, Geophys. Res. Lett., 26, 2175-2178, 1999.

Jin, X., Fiore, A. M., Murray, L. T., Valin, L. C., Lamsal, L. N., Duncan, B., Folkert Boersma, K., De Smedt, I., Abad, G. G., Chance, K., and Tonnesen, G. S.: Evaluating a Space-Based Indicator of Surface Ozone-NOx-VOC Sensitivity Over Midlatitude Source Regions and Application to Decadal Trends, J. Geophys. Res-atmos., 122, 10.1002/2017jd026720, 2017.

Li, J., Lu, K., Lv, W., Li, J., Zhong, L., Ou, Y., Chen, D., Huang, X., and Zhang, Y.: Fast increasing of surface ozone concentrations in Pearl River Delta characterized by a regional air quality monitoring network during 2006–2011, J. Environ. Sci-China, 26, 23-36, 10.1016/s1001-0742(13)60377-0, 2014.

Li, K., Jacob, D. J., Liao, H., Shen, L., Zhang, Q., and Bates, K. H.: Anthropogenic drivers of 2013–2017 trends in summer surface ozone in China, Proc. Natl. Acad. Sci., 116, 422-427, 10.1073/pnas.1812168116, 2018.

Li, K., Jacob, D. J., Shen, L., Lu, X., De Smedt, I., and Liao, H.: Increases in surface ozone pollution in China from 2013 to 2019: anthropogenic and meteorological influences, Atmos. Chem. Phys., 20, 11423-11433, 10.5194/acp-20-11423-2020, 2020.

Li, X.-B., Yuan, B., Parrish, D. D., Chen, D., Song, Y., Yang, S., Liu, Z., and Shao, M.: Long-term trend of ozone in southern China reveals future mitigation strategy for air pollution, Atmos. Environ., 269, 10.1016/j.atmosenv.2021.118869, 2022.

Lin, H., Xing, C., Hong, Q., Liu, C., Ji, X., Liu, T., Lin, J., Lu, C., Tan, W., Li, Q., and Liu, H.: Diagnosis of Ozone Formation Sensitivities in Different Height Layers via MAX‐DOAS Observations in Guangzhou, J. Geophys. Res-atmos., 127, 10.1029/2022jd036803, 2022.

Liu, J., Li, X., Tan, Z., Wang, W., Yang, Y., Zhu, Y., Yang, S., Song, M., Chen, S., Wang, H., Lu, K., Zeng, L., and Zhang, Y.: Assessing the Ratios of Formaldehyde and Glyoxal to NO2 as Indicators of O3–NOx–VOC Sensitivity, Environ. Sci. Technol., 55, 10935-10945, 10.1021/acs.est.0c07506, 2021.

Liu, Y., Geng, G., Cheng, J., Liu, Y., Xiao, Q., Liu, L., Shi, Q., Tong, D., He, K., and Zhang, Q.: Drivers of Increasing Ozone during the Two Phases of Clean Air Actions in China 2013–2020, Environ. Sci. Technol., 57, 8954-8964, 10.1021/acs.est.3c00054, 2023.

Ma, Y., Diao, Y., Zhang, B., Wang, W., Ren, X., Yang, D., Wang, M., Shi, X., and Zheng, J.: Detection of formaldehyde emissions from an industrial zone in the Yangtze River Delta region of China using a proton transfer reaction ion-drift chemical ionization mass spectrometer, Atmos. Meas. Tech., 9, 6101-6116, 10.5194/amt-9-6101-2016, 2016.

Martin, R. V., Fiore, A. M., and Van Donkelaar, A.: Space‐based diagnosis of surface ozone sensitivity to anthropogenic emissions, Geophys. Res. Lett., 31, 10.1029/2004gl019416, 2004.

Ren, J., Guo, F., and Xie, S.: Diagnosing ozone–NOx–VOC sensitivity and revealing causes of ozone increases in China based on 2013–2021 satellite retrievals, Atmos. Chem. Phys., 22, 15035-15047, 10.5194/acp-22-15035-2022, 2022.

Sun, Y., Yin, H., Liu, C., Zhang, L., Cheng, Y., Palm, M., Notholt, J., Lu, X., Vigouroux, C., Zheng, B., Wang, W., Jones, N., Shan, C., Qin, M., Tian, Y., Hu, Q., Meng, F., and Liu, J.: Mapping the drivers of formaldehyde

(HCHO) variability from 2015 to 2019 over eastern China: insights from Fourier transform infrared observation and GEOS-Chem model simulation, Atmos. Chem. Phys., 21, 6365-6387, 10.5194/acp-21-6365-2021, 2021.

Vigouroux, C., Langerock, B., Bauer Aquino, C. A., Blumenstock, T., Cheng, Z., De Mazière, M., De Smedt, I., Grutter, M., Hannigan, J. W., Jones, N., Kivi, R., Loyola, D., Lutsch, E., Mahieu, E., Makarova, M., Metzger, J. M., Morino, I., Murata, I., Nagahama, T., Notholt, J., Ortega, I., Palm, M., Pinardi, G., Röhling, A., Smale, D., Stremme, W., Strong, K., Sussmann, R., Té, Y., van Roozendael, M., Wang, P., and Winkler, H.: TROPOMI–Sentinel-5 Precursor formaldehyde validation using an extensive network of ground-based Fourier-transform infrared stations, Atmos. Meas. Tech., 13, 3751-3767, 10.5194/amt-13-3751-2020, 2020.

Wang, M., Chen, W., Shao, M., Lu, S., Zeng, L., and Hu, M.: Investigation of carbonyl compound sources at a rural site in the Yangtze River Delta region of China, J. Environ. Sci-China, 28, 128-136, 10.1016/j.jes.2014.12.001, 2015.

Wang, Y., Dörner, S., Donner, S., Böhnke, S., De Smedt, I., Dickerson, R. R., Dong, Z., He, H., Li, Z., Li, Z., Li, D., Liu, D., Ren, X., Theys, N., Wang, Y., Wang, Y., Wang, Z., Xu, H., Xu, J., and Wagner, T.: Vertical profiles of NO2, SO2, HONO, HCHO, CHOCHO and aerosols derived from MAX-DOAS measurements at a rural site in the central western North China Plain and their relation to emission sources and effects of regional transport, Atmos. Chem. Phys., 19, 5417-5449, 10.5194/acp-19-5417-2019, 2019.

Wang, Z., Liu, C., Xie, Z., Hu, Q., Andreae, M. O., Dong, Y., Zhao, C., Liu, T., Zhu, Y., Liu, H., Xing, C., Tan, W., Ji, X., Lin, J., and Liu, J.: Elevated dust layers inhibit dissipation of heavy anthropogenic surface air pollution, Atmos. Chem. Phys., 20, 14917-14932, 10.5194/acp-20-14917-2020, 2020.

Xing, C., Liu, C., Wang, S., Chan, K. L., Gao, Y., Huang, X., Su, W., Zhang, C., Dong, Y., Fan, G., Zhang, T., Chen, Z., Hu, Q., Su, H., Xie, Z., and Liu, J.: Observations of the vertical distributions of summertime atmospheric pollutants and the corresponding ozone production in Shanghai, China, Atmos. Chem. Phys., 17, 14275-14289, 10.5194/acp-17-14275-2017, 2017.

Zhai, S., Jacob, D. J., Wang, X., Shen, L., Li, K., Zhang, Y., Gui, K., Zhao, T., and Liao, H.: Fine particulate matter (PM2.5) trends in China, 2013–2018: separating contributions from anthropogenic emissions and meteorology, Atmos. Chem. Phys., 19, 11031-11041, 10.5194/acp-19-11031-2019, 2019.

Zhang, Q., Zheng, Y., Tong, D., Shao, M., Wang, S., Zhang, Y., Xu, X., Wang, J., He, H., Liu, W., Ding, Y., Lei, Y., Li, J., Wang, Z., Zhang, X., Wang, Y., Cheng, J., Liu, Y., Shi, Q., Yan, L., Geng, G., Hong, C., Li, M., Liu, F., Zheng, B., Cao, J., Ding, A., Gao, J., Fu, Q., Huo, J., Liu, B., Liu, Z., Yang, F., He, K., and Hao, J.: Drivers of improved PM2.5 air quality in China from 2013 to 2017, Proc. Natl. Acad. Sci., 116, 24463-24469, 10.1073/pnas.1907956116, 2019.

Zheng, B., Tong, D., Li, M., Liu, F., Hong, C., Geng, G., Li, H., Li, X., Peng, L., Qi, J., Yan, L., Zhang, Y., Zhao, H., Zheng, Y., He, K., and Zhang, Q.: Trends in China's anthropogenic emissions since 2010 as the consequence of clean air actions, Atmos. Chem. Phys., 18, 14095-14111, 10.5194/acp-18-14095-2018, 2018.